15TH IEA HEAT PUMP CONFERENCE
MAY 26–29, 2026 | HOFBURG
VIENNA 2026
DECARBONISATION THROUGH INNOVATION

# Decarbonization of district heating and cooling: Role of seasonal thermal energy storage and heat pumps

Abdulrahman Dahash[a]*, Michael Bayer[b], Mustafa Kalfa[a], Lara Bajlo[a], Reinhard Jentsch[a], Michael Lauermann[a]

[a]Sustainable Thermal Energy Systems, Center for Energy, AIT Austrian Institute of Technology GmbH, 1210 Vienna, Austria
[b]School of Engineering and Architecture, Lucerne University of Applied Sciences and Arts, 6048, Horw, Switzerland

**Abstract**

The decarbonization of district heating (DH) systems requires scalable solutions capable of integrating renewable heat sources while reducing reliance on peak boilers. Seasonal thermal energy storage (sTES) and large-scale heat pumps (HPs) are among the most promising technologies to tackle this challenge, particularly in solar-assisted district heating (S-DH) networks where fluctuating solar heat availability requires flexible thermal management. This study evaluates the combined integration of a large-scale sTES and a water-to-water HP into a representative Austrian DH system, focusing on optimal sTES sizing and the impact of HP placement on system efficiency, solar fraction, reduction on $CO_2$-emissions and operating cost reduction.
A dynamic simulation model of S-DH is developed, incorporating detailed sTES and HP components and a top-level control strategy for operational dispatch. Two sTES technologies; tank (TTES) and pit (PTES), are examined ranging from 210,000 $m^3$ up to 360,000 $m^3$. Three alternative HP integration configurations are compared: (i) HP coupled directly to sTES, (ii) HP upgrading solar heat, and (iii) HP installed on the DH return line.
Findings indicate that TTES provides the best overall performance, with an optimal volume of 330,000 $m^3$ and efficiency of around 90%, while PTES exhibits substantially higher thermal losses and lower efficiencies despite slightly higher solar fractions. Outcomes pinpoint the DH-return configuration with the strongest technical performance, achieving the highest SCOP values and enabling the largest transition from gas-based production. Yet, the direct sTES–HP coupling shows the highest sTES efficiency-around 3% points higher than the other configurations-due to deeper discharge and lower operating temperatures. The DH-integrated HP configuration resulted in the greatest annual OPEX savings, exceeding 35% at high HP capacities.
Hence, detailed design and layout of HP and sTES integration significantly enhances renewable utilization, system efficiency, and cost-effectiveness, providing a clear pathway for next-generation low-carbon district heating systems.



*Keywords: Seasonal thermal energy storage; heat pumps; solar-assisted district heating; sector coupling; planning and integration.*

## 1. Introduction

The transition towards a carbon-neutral energy system is under acceleration worldwide, driven by ambitious policies such as the European Green Deal, which targets at least a 55% reduction in greenhouse gas (GHG) emissions by 2030 compared to 1990 levels [1]. Since space heating and domestic hot water production account for nearly 16 % of total EU GHG emissions [2], the decarbonization of the building sector plays a vital role in achieving these targets. District heating (DH) systems are an efficient and scalable solution for supplying heat in urban areas and offer the flexibility to integrate various renewable and waste heat sources [3] and [4].

The growing share of variable renewable energy sources introduces operational challenges in DH networks, as heat demand and renewable production rarely coincide. Thermal energy storage (TES) is therefore essential

* Corresponding author. *E-mail address:* abdulrahman.dahash@ait.ac.at

for decoupling heat generation from demand, enabling higher renewable integration and improving overall system flexibility [5]. TES reduces the need for fossil-based peak units and allows the exploitation of low-cost or surplus energy, leading to lower operating costs and $CO_2$ emissions [6].

Several seasonal TES concepts are developed for DH systems, including cavern (CTES), tank (TTES), pit (PTES), borehole (BTES), and aquifer (ATES) [7]. Among these, PTES has attracted increasing attention due to its low investment cost (< 27 €/m$^3$ [8]), high efficiency, and scalability for seasonal operation. PTES typically consists of a large water reservoir excavated in the ground, lined with a polymer liner and insulated by a floating lid. In Denmark, PTES technology has been successfully implemented in large solar DH systems, such as Marstal (75,000 m$^3$), Dronninglund (60,000 m$^3$), and Vojens (200,000 m$^3$), achieving solar fractions above 40 % [9].

In addition to sTES integration, heat pumps (HPs) emerge as a key component in renewable-based DH networks. HPs enable the conversion of renewable electricity to heat and can utilize low-temperature sources such as waste heat or sTES. When coupled with an sTES, a HP can operate more efficiently due to the stable temperature environment provided by the storage, while simultaneously enhancing the stratification and usable capacity of the sTES [1]. Depending on the system design, the HP can be located (a) next to the sTES using it as a heat source, (b) coupled to solar thermal collectors for heat injection into DH network, or (c) positioned in the DH network downstream of both technologies.

Although sTES and HP technologies are individually studied in DH systems, the optimal integration strategy and component placement remain open research questions. Previous works focused either on the design and performance of sTES in solar-assisted district heating (S-DH) systems [10], [11] and [12]. Other studies examined the operational optimization of HP-based networks [13], but the combined effects of HP location, storage operation, and solar integration on the system performance are still insufficiently explored.

For instance, Tosatto et al. [1] conducted a techno-environmental analysis focusing on the role of HP and sTES integration into DH systems. The work addressed several key highlights such as the role of HPs in increasing sTES efficiency and capacity and reducing the ground temperature to meet several predefined regulatory thresholds for ground temperature. Yet, the work simplified the system to profile-based representation and the dynamic interaction was not considered due to the use of a component-based multiphysics tool (i.e., COMSOL Multiphysics). On a brighter not, Sifnaios et al. [6] numerically investigated the integration of a HP together with a PTES into an S-DH. The work carried out techno-economic optimization framework with an objective function focusing on the minimization of levelized cost of heat. Yet, the work used PTES technology as a short-term storage technology not seasonal.

Therefore, this study investigates the integration of a large-scale sTES and a HP into an S-DH network to determine the optimal HP location relative to the sTES and solar collector field. A dynamic simulation model of the S-DH system is developed in Modelica/Dymola, incorporating detailed sTES and HP components and a top-level control strategy to minimize system operation cost (OPEX) and $CO_2$-emissions. The analysis aims to quantify the impact of HP placement on system efficiency, renewable utilization, and levelized cost of stored heat, providing design guidelines for next-generation renewable district heating systems.

## 2. Methodology

### *2.1. District heating system*

The case study considers a fictitious large DH network located in Austria, supplying approximately 225,000 inhabitants. The network delivers an annual space heating demand of 333 GWh, with a peak heat load exceeding 150 MW. The system operates at supply temperatures above 80 °C, characteristic of high-temperature fourth-generation DH networks with a mix of existing building stock. The return temperature typically remains around 40 – 45 °C, resulting in a mean temperature difference of approximately 35 – 40 K.

Figure 1 shows the annual variation of heat load, supply temperature, and ambient temperature. The heating demand exhibits an obvious seasonal pattern, with high loads during winter and negligible demand in summer. It is worthy to highlight that the domestic hot water demand is neglected in this work and, thus, Figure 1(a) shows no heat load during summer. The supply temperature follows a weather-compensated curve, decreasing from about 95 °C in cold periods to around 65 °C in summer operation, which meets the supply temperature for domestic hot water demand. The ambient temperature ranges from approximately –15 °C up to 35 °C, clearly influencing both the heat demand. The lowest supply temperature of 65 °C during summer is attributed to the Austrian guidelines to have a minimum temperature of 65 °C for DHW that prevents Legionella. Therefore, Figure 1 shows a supply temperature of 65 °C despite the heat load is 0 during summer months, as the load refers to the space heating load only.

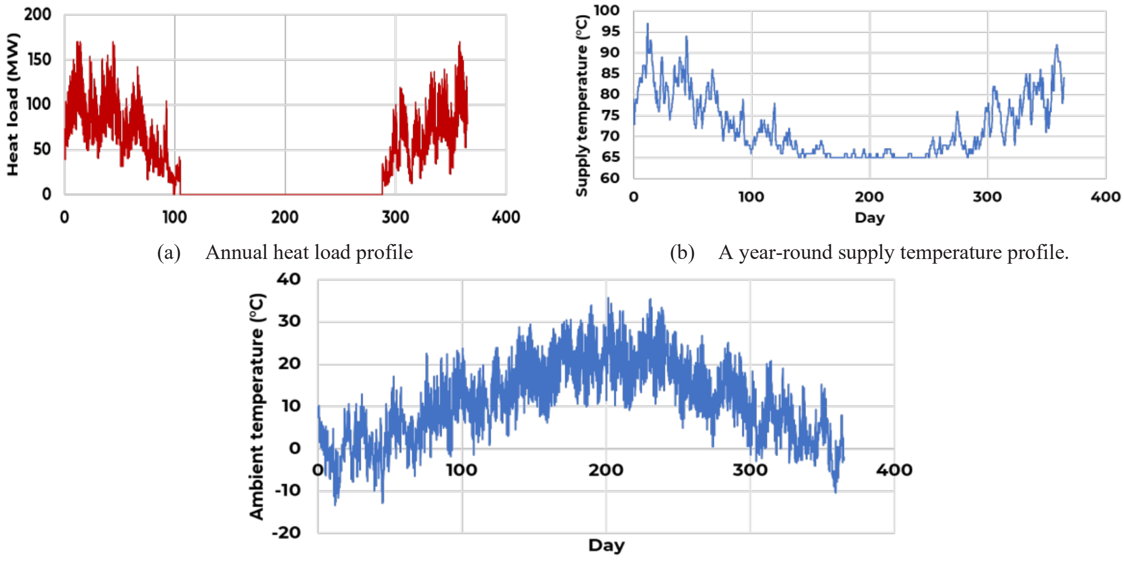


(a) Annual heat load profile

(b) A year-round supply temperature profile.

(c) A year-round ambient temperature profile

Figure 1: Annual profiles for the fictious Austrian district heating system considered in this work.

The existing system mainly relies on gas-fired technologies (i.e. CHPs and peak-boilers) as the base and peak load units. In line with the local decarbonization strategy, the operator considers the integration of large-scale HPs and an sTES technology to increase renewable heat production while maintaining system flexibility and security of supply.

All relevant hourly data – including heat demand, supply and return temperatures, and ambient temperature – are obtained from the DH operator for the reference year 2021. The same profiles were applied for the 25-year simulation horizon to represent long-term operation.

The DH network and its subsystems are modeled dynamically in Modelica/Dymola, using a modular configuration that includes:

- Heat production units: large-scale water-source HPs and peak boiler,
- Solar collector field with a gross area of 76,000 $m^2$ and an average global horizontal irradiance of 1200 $kWh/m^2$, efficiency coefficients are: C0 = 0.77, C1 = 2.1 $W/(m^2 \cdot K)$ and C2 = 0.01 $W/(m^2 \cdot K^2)$,
- seasonal thermal energy storage, and
- Aggregated district heating load.

This setup allows for detailed assessment of HP integration configurations under consistent boundary conditions, evaluating both thermal performance and techno-economic impacts

*2.2. Hydraulic integration of sTES and HP in S-DH system*

The study investigates three alternative configurations for integrating a large-scale HP into the S-DH system, differing in their thermal coupling into the systems:

(a) Configuration A – sTES HP: the HP is connected to the seasonal thermal energy storage sTES circuit. In this layout, the HP utilizes low-temperature heat extracted from the sTES during charging and supplies heat to DH network. This configuration maximizes the synergy between solar energy and the HP by exploiting the sTES as a stable heat source.

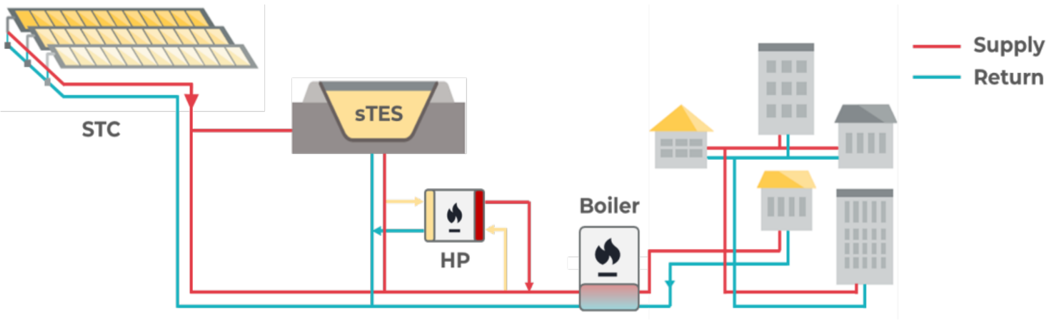


Figure 2: Configuration A highlighting the integration of HP next to the sTES technology for sTES deep discharge.

(b) Configuration B – ST HP: the HP is directly coupled to the solar thermal field and operates when solar irradiation is insufficient to reach DH supply temperatures. The HP upgrades solar heat in real time and injects it into the DH network, while the sTES operates as a seasonal buffer.

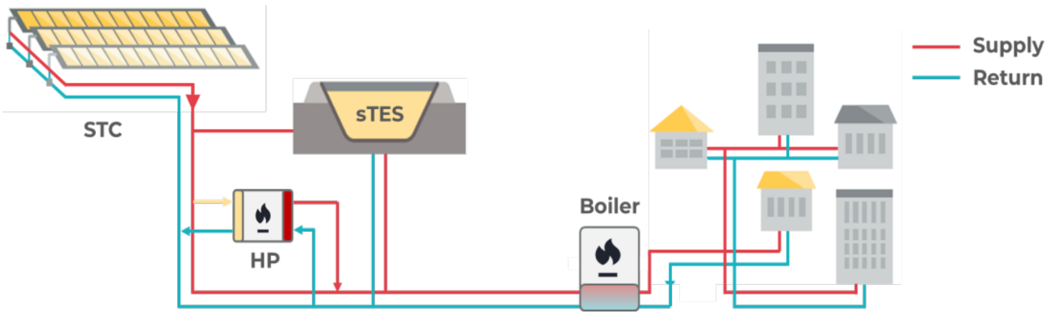


Figure 3: Configuration B highlighting the integration of HP next to the STC to improve output temperature during winter.

(c) Configuration C – DH HP: the HP is integrated on the DH return line, using the return water as a heat source and supplying heat directly to the main supply line. In this configuration, the HP operates independently of the solar field and sTES, representing a conventional approach in high-temperature DH systems.

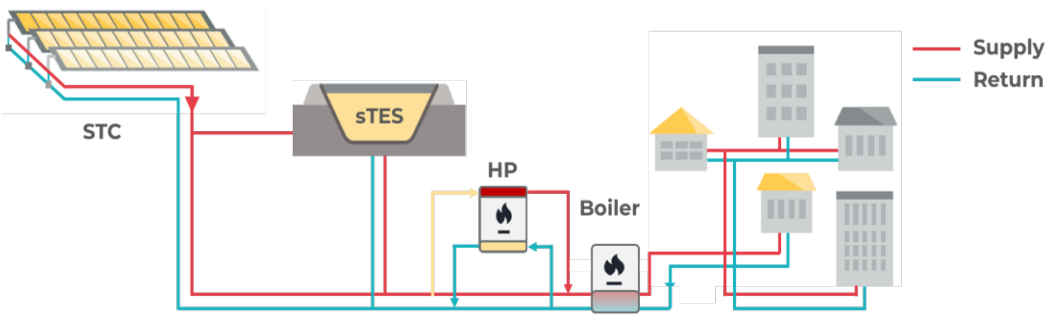


Figure 4: Configuration C highlighting the integration of HP in S-DH network on both return and supply line.

Each configuration is implemented in Modelica/Dymola and simulated under identical boundary conditions and control strategy, allowing a consistent comparative analysis.

### *2.3. sTES design parameters*

In this work, two sTES technologies are considered and that are TTES and PTES systems. Despite the fact that the work investigates the optimal volume of sTES technology for the considered S-DH system, the work will consider the design of PTES based on the design of the Dronninglund PTES, which consists of an inverted truncated pyramid with a height of 16 m. However, the work simulates PTES as an inverted truncated cone instead of an inverted truncated pyramid with a correction factor of the surface area and relevant thermal conductance. Besides, the PTES volume is a variable subject to optimization. Moreover, the PTES is insulated by a floating lid and surrounded by a compacted soil layer.

For the TTES technology, the work will consider the height of TTES is 25 m in the subsurface, while the volume is also subject to optimization. The work considers a lid with no insulation on the sidewalls and bottom for TTES. Table 1 summarizes the relevant design parameters for the different sTES technologies considered in this work.

Table 1: Relevant design parameter for the different sTES investigated in this work.

| **Parameter** | **TTES** | **PTES** |
|---|---|---|
| Height, m | 25 | 16 |
| Slope, ° | 90 | 30 |
| Top radius, m | Subject to optimal size | |
| Bottom radius, m | Subject to optimal size (radius of 0 m is excluded) | |
| Volume, m$^3$ | Subject to optimization | |
| $U_{top}$, W/(m$^2$·K) | 0.15 | |
| $U_{side}$, W/(m$^2$·K) | 90, no insulation | |
| $U_{bottom}$, W/(m$^2$·K) | 90, no insulation | |

### *2.4. Heat pump*

Water-to-water heat pumps are selected due to their flexibility, scalability, and broad applicability in the Danish S-DH systems. Herein, the HP is emulated as a dynamic system whose COP varies with the evaporator and condenser temperatures in the same manner as the Carnot efficiency. The control input to the model is the condenser outlet temperature setpoint, which is maintained precisely at steady-state conditions provided that the HP has sufficient capacity.

The nominal heating capacity of a single HP unit is subject to optimization ranging from 2 MW up to 12 MW, and multiple HP units can be aggregated to meet system demand. Thus, detailed refrigeration cycle simulations are not the focus of this work. The coefficient of performance (COP) depends on Carnot efficiency and the temperature lift as expressed below:

$$\mathrm{COP} = \eta_{\mathrm{Carnot}} \cdot \frac{T_{\mathrm{cond,out}}}{T_{\mathrm{cond,out}} - T_{\mathrm{evap,in}}} \cdot y_{\mathrm{PL}} \quad (1)$$

Where $T_{\mathrm{cond,out}}$ and $T_{\mathrm{evap,in}}$ represent the condenser outlet and evaporator inlet temperature, respectively; their difference denotes the temperature lift delivered over the heat pump, whereas ($y_{\mathrm{PL}}$) represents the part-load factor of the heat pump that accounts for changes in in COP during part load operation. This study assumes the HP will be in full-load operation with a Carnot efficiency of 50% for water-source HPs. The performance map of the considered HP is illustrated in Figure 5.

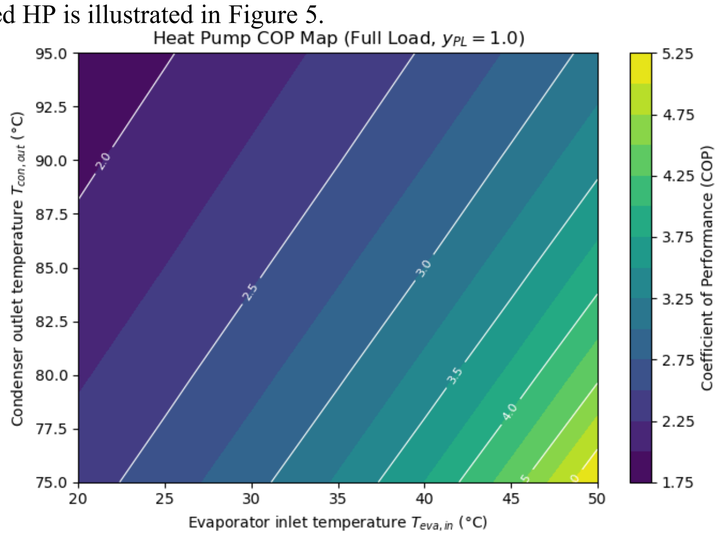


Figure 5: Performance map of the water-source HP unit considered in this work with a nominal heating capacity of 2 MW, part-load factor of 1 and Carnot efficiency of 50%.

### *2.5. Key performance indicators*

Three main key performance indicators (KPIs) are defined to evaluate the system performance and to compare the different configurations. Among these, the sTES efficiency represents a key metric, quantifying the ratio between the discharged and charged thermal energy of the storage over one annual cycle. This indicator is particularly useful for identifying the optimal storage size and volume, as it reflects the effectiveness of energy recovery from the stored heat.

The solar fraction is another crucial KPI, expressing the share of solar energy delivered to the S-DH network (both directly and via the sTES) relative to the total annual space heating demand. A higher solar fraction indicates improved utilization of renewable solar energy and supports the selection of the most suitable sTES type and capacity.

Regarding the integration of HPs, the seasonal coefficient of performance (SCOP) is evaluated to assess their overall energy efficiency under varying operating conditions. This indicator, in combination with the aforementioned KPIs, enables the optimal selection of both HP capacity and system configuration. Finally, the avoidable $CO_2$-emissions is evaluated as an environmental KPI, comparing the investigated S-DH configurations to a reference system without solar and storage integration. This provides an additional perspective on the sustainability and decarbonization potential of each configuration. Further details can be found in Table 2

Table 2: List of the KPIs used in the analysis framework adopted in this work [11].

| KPI | Equation | |
|---|---|---|
| sTES efficiency | $\eta_{\text{sTES}} = \frac{Q_{\text{dis}}}{Q_{\text{ch}}} = \frac{Q_{\text{sTES}\rightarrow\text{S-DH}}}{Q_{\text{STC}\rightarrow\text{sTES}}}$ | (2) |
| Solar fraction | $\text{SF} = \frac{Q_{\text{STC}\rightarrow\text{S-DH}} + Q_{\text{STC}\rightarrow\text{sTES}}}{Q_{\text{SH}}}$ | (3) |
| Seasonal coefficient of performance | $\text{SCOP} = \frac{Q_{\text{HP}\rightarrow\text{S-DH}}}{P_{\text{el}}}$ | (4) |

### *2.6. Economic and environmental assumptions*

In this study, an emission factor of 249 $\text{kg}_{\text{CO2}}/\text{MWh}_{\text{gas}}$ is assumed for natural gas, while the Austrian electricity mix is represented with an emission factor of 69 $\text{kg}_{\text{CO2}}/\text{MWh}_{\text{el}}$. Furthermore, a $CO_2$-tax of 55 €/$\text{ton}_{\text{CO2}}$ is applied. The cost assumptions for energy carriers are 130 €/MWh for natural gas and 200 €/MWh for electricity purchased from the grid.

## 3. Results and discussion

### *3.1. Reference DH system*

For the purposes of this study, the reference DH system is modeled using a single representative, conventional fossil-based technology that aggregates all heat supply units as shown in Figure 6. This technology runs on natural gas with an average efficiency of 90% and offers flexibility in operation, adjusting to the demand for heat based on time and external conditions. The flexibility of the system allows for adjusting the heat output based on real-time requirements and external factors, such as ambient temperature or peak demand times.

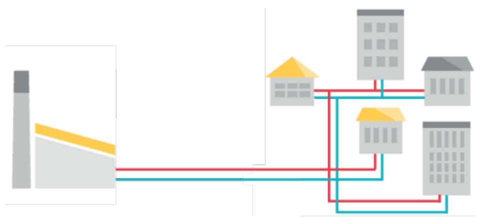

Figure 6: Schematic illustration of reference DH system whereby the space heating demand is met via conventional technologies.

Therefore, the total energy required to meet the heating demand was approximately 333 GWh. Given the average efficiency of 90% for the heat supply units, the energy input of natural gas required for the system to deliver this energy is approximately 370 GWh. This figure accounts for the energy losses in the boiler, meaning that more gas is consumed than the energy delivered as heat. As the combustion of natural gas results in $CO_2$-emissions, the total $CO_2$-emissions for the system are estimated at 92,130 $ton_{CO2}$/a based on an emission factor of 249 $kg_{CO2}/MWh_{gas}$. This represents the carbon footprint of the reference DH system when supplying the space heating demand.

To quantify the cost of $CO_2$-emissions, the applicable carbon tax of 55 €/$ton_{CO2}$ was used. This results in a tax cost of approximately €5,067,150 for the $CO_2$-emissions generated by the system. This cost comes under annual OPEX and it adds a financial burden to the conventional fossil-based DH system, reflecting the importance of considering carbon emissions in the economic evaluation of energy systems.

These calculations highlight the significant environmental and economic costs associated with using a conventional natural gas-based DH system. As the system relies on fossil fuels, its high $CO_2$-emissions and associated carbon tax costs underline the need for exploring alternative, low-carbon technologies, particularly as global carbon pricing and emissions regulations evolve.

### *3.2. Impact of sTES type and size on S-DH*

Herein, the analysis focused the evaluation evaluating the impact of the type and size of sTES on the overall performance of the investigated S-DH system. Two storage concepts were compared: a TTES and a PTES. For each concept, the total storage volume varied between 210,000 m³ and 360,000 m³, whereas the gross area of solar thermal field kept constant with 76,000 m².

Both storage concepts showed a clear increase in the solar fraction with larger storage volumes as shown in Figure 7. This trend is expected, as higher volumes enable the system to accumulate surplus solar energy during periods of high irradiation and utilize it later in the heating season. For TTES at smaller volumes (around 210,000 m³), the solar fraction was relatively low, but it increased significantly as the volume increased leading to a peak at the optimal volume of 330,000 m³. While PTES showed some increase in solar fraction with volume compared to its counterpart, this improvement is marginal as it is around 1% more solar fraction. In this context, PTES provided a higher solar fraction at all tested volumes, but this does not necessarily imply that PTES is more efficient. It rather highlights the fact that the surface area of PTES technologies is larger than that of TTES resulting into more thermal losses and, thus, more accommodation of solar heat. However, the increase rate in solar fraction gradually declined beyond approximately 300,000 m³, indicating relatively weak economic returns with further sTES enlargement.

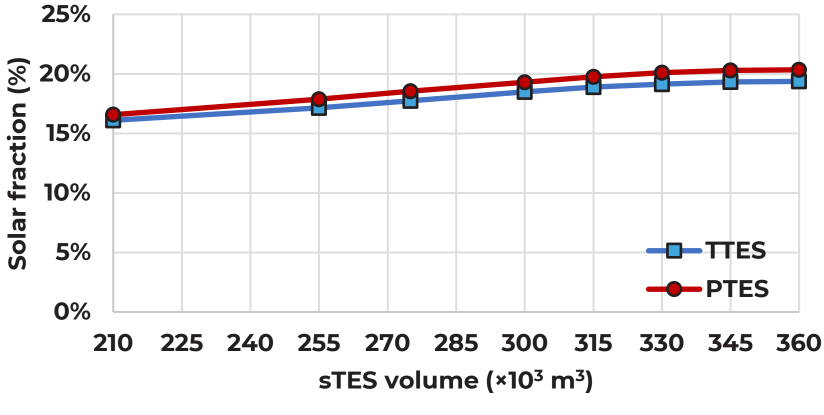


Figure 7: Solar fraction vs. sTES volume considered in this work.

Figure 8 presents the sTES efficiency across the different volumes investigated and, therein, it is obvious that sTES efficiency followed a similar pattern to the solar fraction. Across the entire volume range, TTES exhibited efficiencies between 80% and 90%, whereas PTES achieved 57–76%. Subsequently, TTES efficiency showed a clear upward trend with volume, achieving its highest efficiency at a volume of 330,000 m³. Beyond this point, the increase in efficiency was minimal, implying that the system had reached its optimal operating conditions. While PTES showed a more gradual increase in efficiency with volume, its rate of improvement accelerated significantly at higher volumes unlike that rate in solar fraction. Yet, marginal gains in PTES efficiency observed past the volume of 330,000 m³.

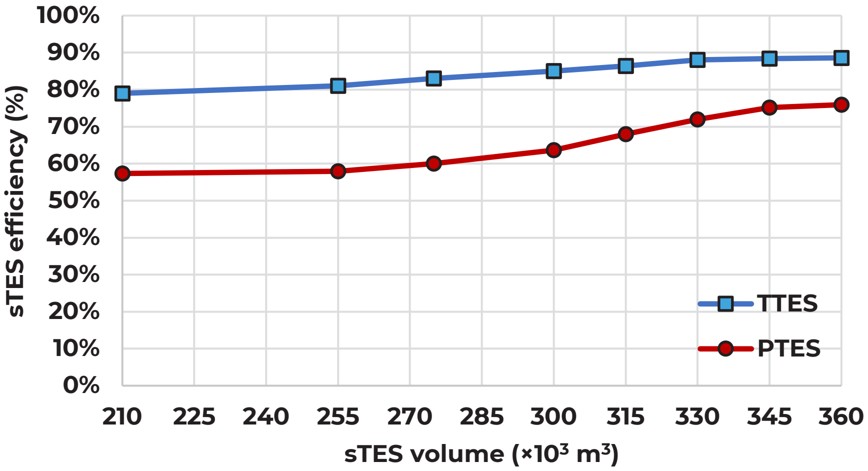


Figure 8: sTES efficiency vs. sTES volume considered in this work.

By analyzing the trade-off between the solar fraction gain and the marginal efficiency improvement with increasing volume, the optimal configuration was identified as the TTES with a total volume of 330,000 m³. At this size, the storage provides a favorable balance between system performance and investment requirements, maximizing the renewable contribution without significant over-dimensioning. Although the PTES could offer lower construction costs, the associated heat losses reduce its annual efficiency and solar utilization potential, making the TTES the preferred solution for the investigated district heating network.

Furthermore, Figure 9 supports the conclusion that TTES with a total volume of 330,000 m³ is the optimal choice. Therein, it is obvious that TTES continues to outperform PTES across various volumes, with significant improvements the avoidable amount of $CO_2$-emissions that can be translated into less use of gas-fired boilers. Besides, the outcomes show a clear peak at 330,000 m³ for TTES, after which further increases in volume offer diminishing returns in terms of performance.

Due to higher sTES efficiency and improved overall system performance demonstrated by TTES, this clearly emerges as the more suitable sTES option for the investigated S-DH system. The TTES configuration achieves an efficiency of approximately 90% and exhibits stable behavior across the entire volume range, while PTES consistently underperforms due to elevated ground heat losses despite marginally higher solar fractions. Consequently, the subsequent analysis of HP integration is carried out using a TTES with a volume of 330,000 m³, as it represents the most technically robust and energy-efficient solution.

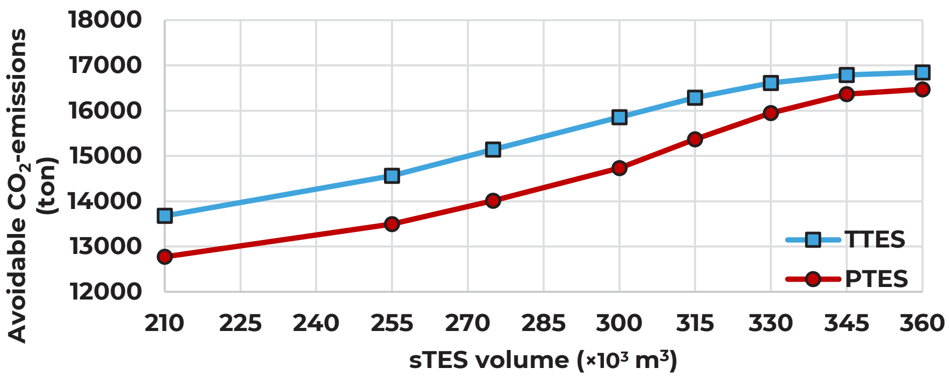


Figure 9: Avoidable amount of $CO_2$-emissions vs. sTES volume considered in this work

*3.3. Impact of HP integration*

The integration of HPs into S-DH equipped with sTES systems is pivotal for performance optimization of these networks. The effectiveness of such integration depends on the interaction between the heat pump capacity, sTES storage characteristics, and the overall system efficiency. Figure 10 presents various performance metrics – heat pump output, SCOP, solar fraction, and sTES efficiency – across different HP integration capacities to highlight the impact of HP integration on system performance.

Figure 10(a) shows the relationship between HP capacity and the total HP output for the three configurations considered in this work. Therein, all configurations exhibit an increase in HP output with larger HP capacities, suggesting the linear relationship between output and capacity. However, it is worthwhile to mention that the DH HP configuration (Configuration C) consistently demonstrates higher HP output compared to its counterparts (both Configuration A and B) at equivalent capacities. This is because the HP is integrated into the network and can take advantage of return temperature and uses the return line as source while boosting the supply temperature. The decrease in return temperature leads to higher STC efficiency. Hence, this allows for further accumulation of surplus solar thermal energy and its subsequent release during the heating season.

Figure 10(b) presents the SCOP as a function of HP capacity for each configuration. SCOP decreases slightly with increasing heat pump capacity, which is a typical trend due to declining returns in efficiency at larger capacities. Notably, the DH HP configuration (Configuration C) maintains the highest SCOP across all tested capacities, with values nearly 3.0. In contrast, the ST HP configuration (Configuration B) exhibits the lowest SCOP values, especially at higher heat pump capacities. This can be attributed to the low outlet temperatures from ST collectors during winter periods that lead to a negative impact on SCOP. Moreover, tis outcome suggests that while larger HP capacities yield higher energy outputs, the SCOP tends to decrease as the system is scaled up. The decline in SCOP can be attributed to the increased temperature lift, which may offset the performance gains from increased output.

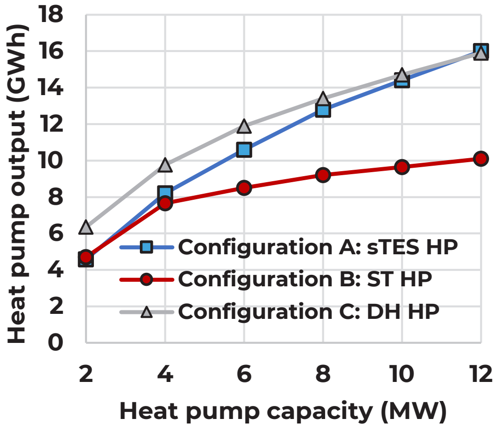


(a) Annual heat pump output

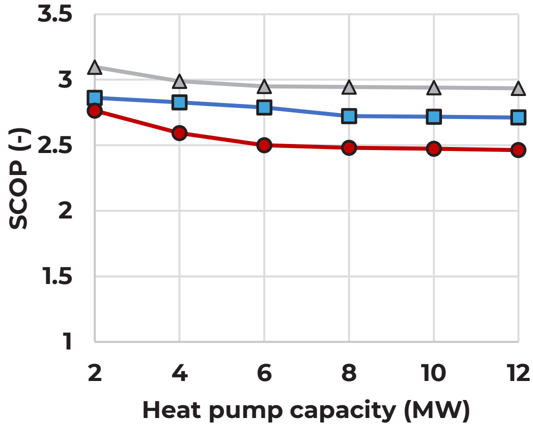


(b) SCOP

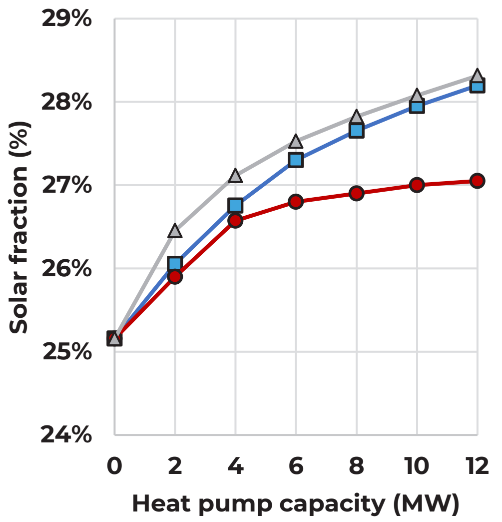


(c) Solar fraction

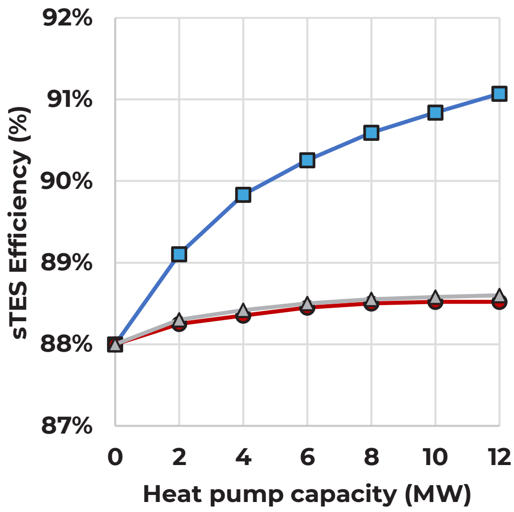


(d) sTES efficiency

Figure 10: Technical comparative analysis of the three configurations for HP integration considered in this work.

Figure 10(c) illustrates the solar fraction as a function of HP capacity. Therein, a clear positive trend in solar fraction can be observed as HP capacity increases, with the DH HP configuration again leading in solar contribution. At higher capacities, the system can store and utilize more solar energy, reducing the reliance on auxiliary heating sources. While the sTES HP and ST HP configurations show substantial increases in solar fraction, the DH HP configuration exhibits a more moderate improvement. Yet, it is worthwhile to pinpoint that the configuration sTES HP shows relatively similar solar fraction values compared to DH HP configuration at HP capacity beyond 6 MW. This is due to the larger sTES capacity associated with the sTES HP, which allows for the accumulation of more solar thermal energy and its later release during winter. This result emphasizes the role of the sTES in enhancing HP performance by providing a stable and reliable thermal buffer, which is especially important during periods of low solar irradiation.

Figure 10(d) shows the sTES efficiency as a function of HP capacity. Therein, it is obvious that sTES efficiency increases with HP capacity. Yet, this increase is less pronounced for both configurations (Configuration B and C) compared to its counterpart A. The latter (Configuration A) demonstrates the highest efficiency across the full range of capacities, with values approaching 91%. This increase in efficiency is attributed to the larger storage capacity available in the sTES HP configuration. The lower storage temperatures achieved in this configuration enhance the potential for beneficial heat gains from the surrounding subsurface.

In contrast, the efficiency observed in the DH–HP (Configuration B) and ST–HP (Configuration C) remain lower because the sTES operating conditions are not modified relative to the baseline S-DH case. As a result, these configurations experience comparatively higher thermal losses and less effective utilization of the stored energy, limiting the overall sTES performance despite the increase in HP capacity.

Figure 11 presents the annual $CO_2$-emissions reduction achieved by the three configurations as a function of installed HP capacity, benchmarked against the gas-fired CHP reference case (83,000 $ton_{CO2}$/a). All configurations exhibit a clear trend of increasing $CO_2$-emissions savings with higher HP capacity, indicating the progressive transition from gas-based heat production to solar-assisted, electricity-driven heat generation.

Configuration C (DH HP) brings the highest $CO_2$-emissions reduction across the entire capacity range, reaching values above 31% at 12 MW. This is driven by the configuration's advantageous thermal integration, which enables a higher share of heat generation to be shifted from the gas-fired CHPs to the HP even at moderate capacities. Configuration A (sTES HP) shows consistently strong reductions as well, achieving nearly 31% at 12 MW. Although slightly lower than Configuration C, its improvements remain significant and nearly parallel in trend due to the increased utilization of low-temperature solar heat and the reduction of losses enabled by the expansion of sTES capacity.

In contrast, Configuration B (ST HP) yields consistently lower reductions with marginal improvements beyond a capacity of 4 MW. This reveals the limited impact of HP herein on shifting heat production, where storage operating conditions remain less favorable for maximizing the substitution of gas-fired operation. Overall, the results highlight that while all three alternatives reduce emissions meaningfully, the DH HP configuration offers the highest potential for decarbonization.

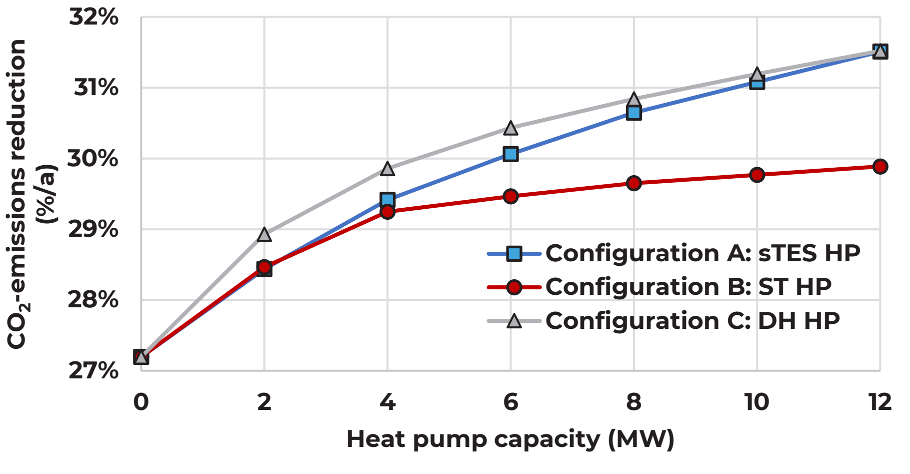


Figure 11: $CO_2$-emissions reduction vs. installed heat pump (HP) capacity for the three configurations considered in this work.

Figure 12 reports the annual savings in OPEX compared to the gas-fired reference system. In all configurations, OPEX savings increase with HP capacity due to reduced gas consumption and associated $CO_2$-related taxing costs. Configuration C (DH HP) provides the highest savings at lower capacities, owing to its favorable integration in the DH network. At larger capacities, however, Configuration A (sTES HP) slightly overtakes it, reaching almost 14 million €/a at 12 MW. This improvement stems from the enhanced utilization of sTES and expansion of its capacity, which enable deeper reductions in conventional heat production.

Configuration B (ST HP) shows the lowest savings across the entire capacity range, as its integration leads to smaller shifts in system operation and thus less gas and $CO_2$-emissions avoidance. Overall, all configurations yield notable OPEX reductions, with the sTES-coupled HP arising as the most advantageous option at higher capacities.

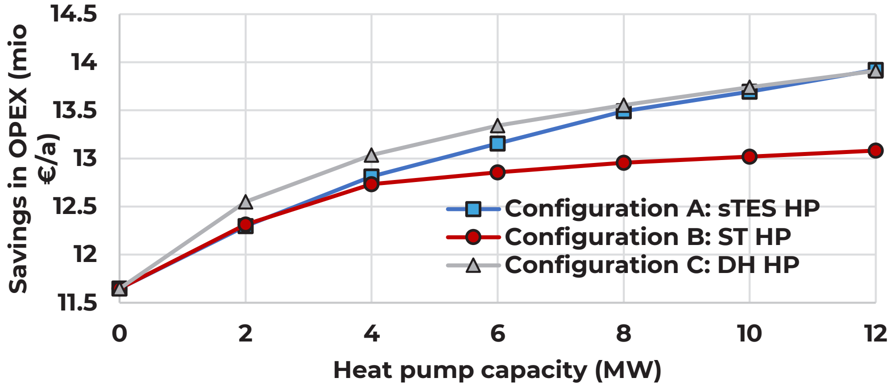


Figure 12: Annual OPEX savings relative to the gas-fired reference case vs HP capacity, considering fuel, electricity, and $CO_2$-emissions costs.

## Conclusions

The decarbonization of district heating (DH) systems relies on the integration of efficient, flexible, and low-carbon technologies. In this context, large-scale heat pumps (HPs) and seasonal thermal energy storage (sTES) play a central role, as they enable low-temperature operation, facilitate renewable integration, and reduce reliance on conventional heat generation. Solar-assisted district heating (S-DH) concepts in particular benefit from the synergistic interaction between HPs, solar thermal production, and sTES, allowing for improved utilization of variable renewable heat and enhanced operational resilience.

This work demonstrated the role of HPs and sTES in the heat transition. With the aid of numerical simulations, the comparative assessment of three system configurations showed that the network-integrated heat pump (configuration C) exhibited the strongest technical performance across the evaluated HP capacities under the considered boundary conditions. Furthermore, the direct sTES-HP coupling (configuration B) emphasized the advantage of coupling HP with sTES: the sTES can be discharged substantially below the return temperature of the S-DH system, expanding the effective storage capacity and lowering thermal losses. This behavior increased the sTES energy efficiency by more than 3% points compared with configurations where the HP is not directly linked to the sTES.

Regarding economic performance, the integration of the HP at the DH return line also proved most advantageous. This configuration yielded the highest annual OPEX savings exceeding €13.5 million per year for the largest HP capacity. This is because the return-line integration enabled consistently lower HP lift, increases solar collector efficiency, and allows slightly higher charging of the sTES. Meanwhile, configurations relying on solar-thermal-only charging showed marginal savings as the HP capacity increased.

Overall, the results confirmed that combining large heat pumps with sTES is a highly effective strategy for advancing the heating transition in S-DH systems. While directly coupling the HP to the storage maximizes storage efficiency, integrating the HP into the DH network delivers the most balanced and economically favorable performance. Together, these findings underscore the importance of coordinated HP–sTES design to unlock both technical and economic benefits in future low-carbon district heating systems.

## Nomenclature

| Symbol | Description | Symbol | Description |
|---|---|---|---|
| COP | Coefficient of performance, (-) | $Q_{STC -> sTES}$ | Heat from solar thermal into sTES, (MWh) |
| $P_{el}$ | Electrical input to HP, (MWh) | $Q_{sTES -> S\text{-}DH}$ | Heat injected from sTES into S-DH, (MWh) |
| $Q_{ch}$ | Charged thermal energy in sTES, (MWh) | SCOP | Seasonal coefficient of performance, (-) |
| $Q_{dis}$ | Discharged thermal energy from sTES, (MWh) | SF | Solar fraction, (%) |
| $Q_{HP -> S\text{-}DH}$ | Heat supplied by HP into S-DH network, (MWh) | $T_{cond,out}$ | Temperature at condenser outlet, (K) |
| $Q_{SH}$ | Space heating demand, (MWh) | $T_{evap,in}$ | Temperature at evaporator inlet, (K) |
| $Q_{STC -> S\text{-}DH}$ | Heat injected from solar thermal to network, (MWh) | $y_{PL}$ | Part-load factor, (%) |

**Acknowledgements**

The present study is financially supported by the EU Horizon Europe project INTERSTORES (project No. 101136100).Views and opinions expressed are however those of the author(s) only and do not necessarily reflect those of the European Union or Research Executive Agency. Neither the European Union nor the granting authority can be held responsible for them.

**References**

[1] A. Tosatto, A. Dahash and F. Ochs, "Simulation-based performance evaluation of large-scale thermal energy storage coupled with heat pump in district heating systems," *Journal of Energy Storage,* vol. 61, 2023.

[2] X. Seront, R. Fernandez, N. Mandl and E. Rigler, "Annual European Union greenhouse gas inventory 1990–2020 and inventory report 2022," European Environment Agency (EEA), 2022.

[3] H. Lund, B. Möller, B.V. Mathiesen and A. Dyrelund, "The role of district heating in future renewable energy systems," *Energy,* vol. 35, no. 3, pp. 1381-1390, 2010.

[4] H. Lund, P. A. Østergaard, T. B. Nielsen, S. Werner, J. E. Thorsen, O. Gudmundsson, A. Arabkoohsar and B. V. Mathiesen, "Perspectives on fourth and fifth generation district heating," *Energy,* vol. 227, 2021.

[5] M. Capone, E. Guelpa, G. Mancò and V. Verda, "Integration of storage and thermal demand response to unlock flexibility in district multi-energy systems," *Energy,* vol. 237, 2021.

[6] I. Sifnaios, J. Fan and A. R. Jensen, "Integration of pit thermal energy storages into district heating networks – a techno-economic case study," *Applied Thermal Engineering,* vol. 279, no. Part D, 2025.

[7] C. Bott, I. Dressel and P. Bayer, "State-of-technology review of water-based closed seasonal thermal energy storage systems," *Renewable and Sustainable Energy Reviews,* vol. 113, 2019.

[8] T. Schmidt, T. Pauschinger, P. A. Sørensen, A. Snijders, R. Djebbar, R. Boulter and J. Thornton,, "Design Aspects for Large-scale Pit and Aquifer Thermal Energy Storage for District Heating and Cooling," *Energy Procedia,* vol. 149, pp. 585-594, 2018.

[9] A. Dahash, F. Ochs, M. Bianchi Janetti and W. Streicher, "Advances in seasonal thermal energy storage for solar district heating applications: A critical review on large-scale hot-water tank and pit thermal energy storage systems," *Applied Energy,* vol. 239, pp. 296-315, 2019.

[10] A. Dahash, F. Giordano and A. Serageldin, "Enhancing efficiency and feasibility of large-scale thermal energy storage in district heating," in *Proceedings of BauSim Conference 2024: 10th Conference of IBPSA-Germany and Austria*, Vienna, Austria, 23-26 September 2024.

[11] A. Dahash, F. Ochs and A. Tosatto, "Techno-economic and exergy analysis of tank and pit thermal energy storage for renewables district heating systems," *Renewable Energy,* vol. 180, pp. 1358-1379, 2021.

[12] K. O'Donovan, B. Falay and I. Leusbrock, "Renewables, storage, intelligent control: how to address complexity and dynamics in smart district heating systems?," *Energy Procedia,* vol. 149, pp. 529-538, 2018.

[13] K. Kontu, S. Rinne and S. Junnila, "Introducing modern heat pumps to existing district heating systems – Global lessons from viable decarbonizing of district heating in Finland," *Energy,* vol. 166, pp. 862-870, 2019.